Captive Aerosol Growth and Evolution (CAGE) chamber system to investigate particle growth due to secondary aerosol formation

Candice L. Sirmollo[1,2], Don R. Collins[1,2], Jordan M. McCormick[3], Cassandra F. Milan[3], Matthew H. Erickson[4], James H. Flynn[4], Rebecca J. Sheesley[5], Sascha Usenko[5], Henry W. Wallace[6], Alexander A. T. Bui[6], Robert J. Griffin[6], Matthew Tezak[7], Sean M. Kinahan[7,9], Joshua L. Santarpia[8]

[1]Department of Chemical and Environmental Engineering, University of California Riverside, Riverside, California 92521 USA
[2]College of Engineering, Center for Environmental Research and Technology (CE-CERT), University of California Riverside, Riverside, California 92507 USA
[3]Department of Atmospheric Sciences, Texas A&M University, College Station, Texas 77843 USA
[4]Department of Earth and Atmospheric Sciences, University of Houston, Houston, Texas 77204 USA
[5]Department of Environmental Science, Baylor University, Waco, Texas 76798 USA
[6]Department of Civil and Environmental Engineering, Rice University, Houston, Texas 77005 USA
[7]Sandia National Laboratory, Albuquerque, New Mexico 87123 USA
[8]Department of Pathology and Microbiology, University of Nebraska Medical Center, Omaha, Nebraska 68198 USA
[9]Biodefense and Health Security, University of Nebraska Medical Center, Omaha, Nebraska 68198 USA

Correspondence to: Don R. Collins (donc@ucr.edu)

Supplement

Figure S1. First generation CAGE chambers, which were referred to as QUALITY chambers in some publications.

Figure S2. Close-up photo of a CAGE chamber highlighting the overall clarity.

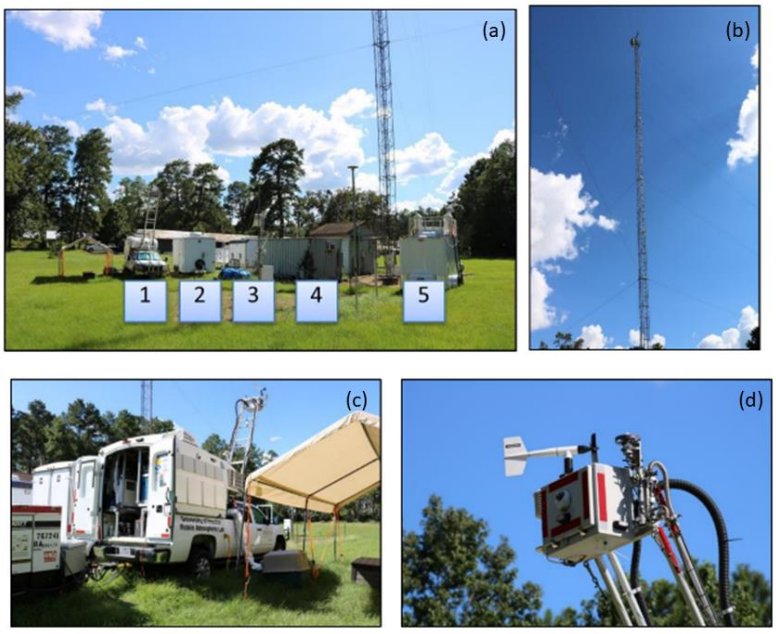

Figure S3. Pictures of MAQL instrumentation and research trailer setup at JSF during field campaign. (a): JSF sampling site within an open clearing of the forest facing southwest, where the following are shown from left to right and are numbered from 1 to 5: (1) University of Houston/Rice University MAQL, (2) Sandia National Laboratories trailer, (3) Texas A&M University trailer, (4) University of Houston/Rice University secondary trailer, and (5) Baylor University trailer, (b): TCEQ CAMPS698 tower located at the site from which wind speed and wind direction data are collected, (c): MAQL showing access to the rear instrumentation bed, and (d): Trace gas/meteorology/PM_1 sampling arm of the MAQL while in stationary sampling mode. Reprinted from Fig S 29 in Alexander Bui's PhD thesis 2018.

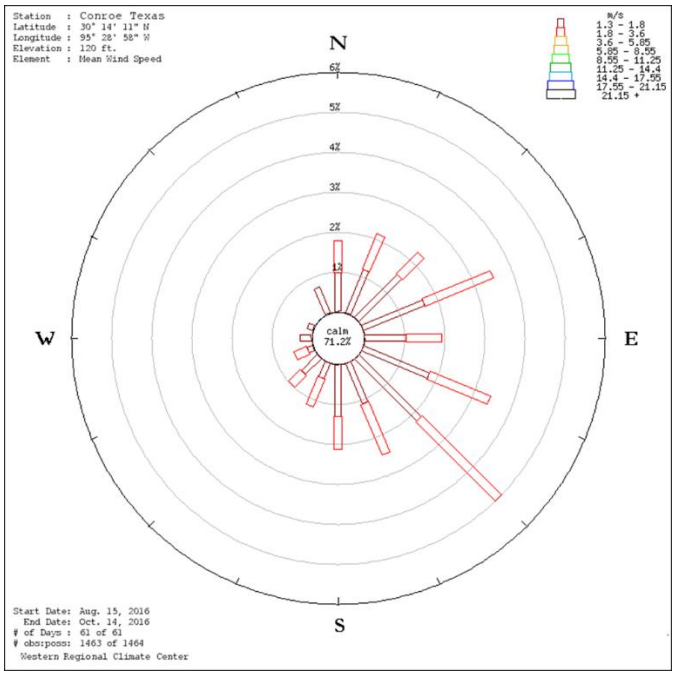

Figure S4. Wind rose calculated for the period of the field study (August 15 – October 14, 2016) at the nearby Conroe airport. Courtesy of the Western Regional Climate Center (wrcc.dri.edu).

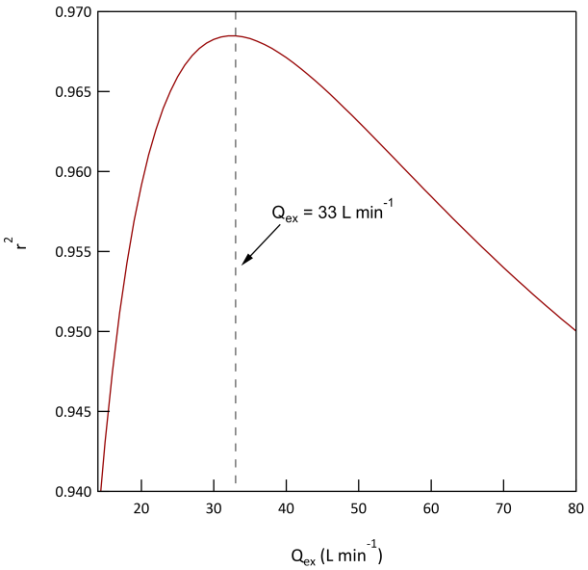

Figure S5. Relationship of the correlation between time series of NO_y concentration i) measured in the chambers and ii) determined from the ambient measurements assuming the chambers can be modeled as CSTRs with exchange flow rate Q_{ex}. The Q_{ex} used for all subsequent calculations is that at which r^2 was highest. The average of the results for Chambers A and B is shown.

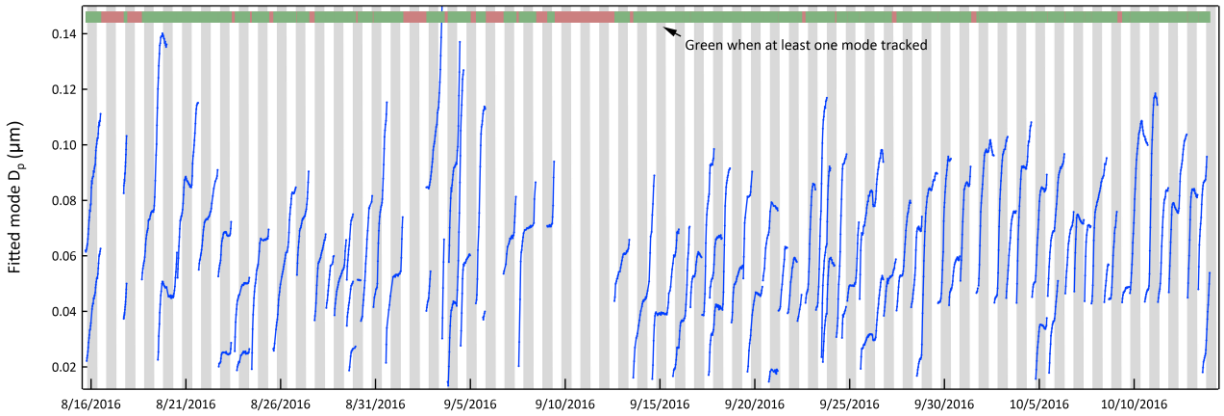

Figure S6. Time series of lognormal fit diameter to all modes tracked during the 2016 study. The color bar towards the top of the graph indicates the periods during which at least one mode was tracked and growth rate could be determined. The gap from 9/9/2016 to 9/12/2016 was the three-day gas-phase comparison experiment discussed in Sect. 4.1.

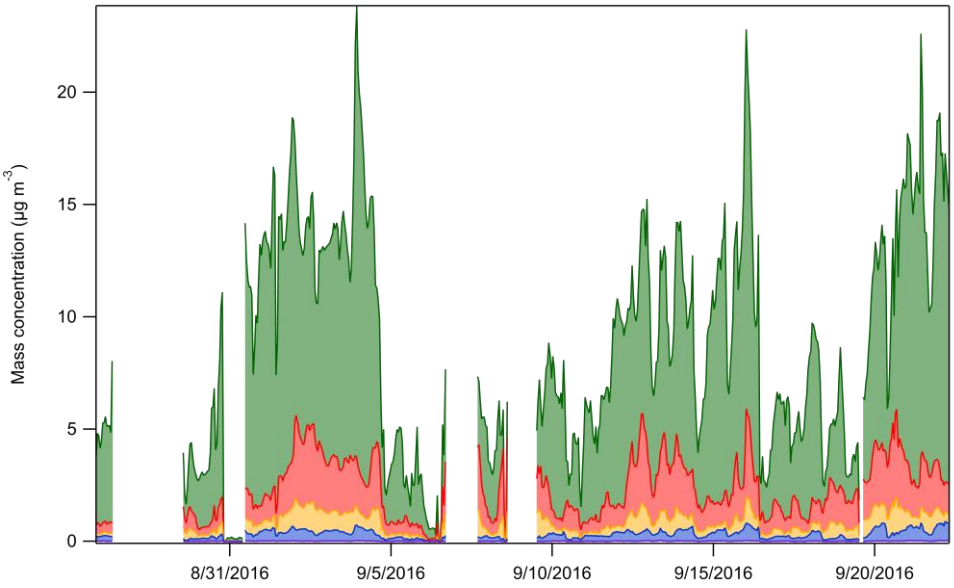

Figure S7. Sub-1 µm non-refractory composition of ambient aerosol measured with an HR-ToF-AMS. The colors indicate the following species: green = organics, red = sulfates, yellow = ammonium, and blue = nitrates.

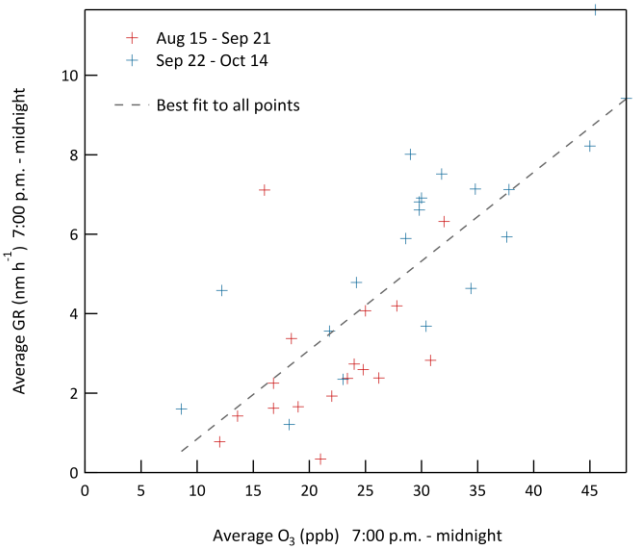

Figure S8. Relationship between the early evening average growth rate and average O_3 mixing ratio. The correlation between the two and the general increase in both during the fall suggests that some of the increased nighttime particle growth towards the end of the project was associated with increased O_3.

Table S1. Reactions included in the CSTR-0D model

Reaction	**Rate coefficient (cm^3 s^{-1} unless stated otherwise)**	**Notes**
$NO + O_3 \rightarrow NO_2 + O_2$	$1.40 \times 10^{-12} \exp(-1310/T)$	
$NO_2 + O_3 \rightarrow NO_3\cdot + O_2$	$1.40 \times 10^{-12} \exp(-2470/T)$	

$NO_2 + NO_3\cdot$ (+ M) → N_2O_5	$1.9 \times 10^{-12} (T/300)^{0.2}$	High pressure limit rate constant and expression
N_2O_5 + M → $NO_2 + NO_3\cdot$	$1.30 \times 10^{-3} (T/300)^{-3.5} \exp(-11000/T)$	
$NO_3\cdot + NO \rightarrow 2NO_2$	$1.80 \times 10^{-11} \exp(110/T)$	
$OH\cdot + NO$ (+ M) → HONO	$1.50 \times 10^{-11} (T/300)^{-0.5}$	High pressure limit rate constant and expression
$OH\cdot + NO_2$ (+ M) → HNO_3	$2.40 \times 10^{-11} (T/300)^{-1.3}$	High pressure limit rate constant and expression
$NO_3\cdot + RO_2\cdot \rightarrow NO_2$	2.00×10^{-12}	
$RO_2\cdot + RO_2\cdot$ → products	2.00×10^{-12}	
$OH\cdot$ + acetaldehyde → $RO_2\cdot$	$5.55 \times 10^{-12} \exp(287/T)$	
Photolysis reactions		
$NO_2 + h\nu \rightarrow NO + O_3$	J_{NO2}	Calculated assuming photostationary state for ambient NO, NO_2, and O_3 concentrations
$NO_3\cdot + h\nu \rightarrow 0.12NO + 0.88NO_2 + 0.88O_3$	J_{NO3}	Calculated from measured spectral intensity
$O_3 + h\nu \rightarrow 0.3OH\cdot + O_3$	J_{O1D}	Calculated from measured spectral intensity. Assumes 15% of $O(^1D)$ produced reacts with H_2O to form $OH\cdot$. O_3 is conserved because any shift this would cause would be captured in the estimated J_{NO2}.
$HONO + h\nu \rightarrow OH\cdot + NO$	J_{HONO}	Calculated from measured spectral intensity
Secondary aerosol forming reactions		
$OH\cdot$ + α-pinene → $RO_2\cdot$	$2.54 \times 10^{-11} \exp(410/T)$	
$OH\cdot$ + β-pinene → $RO_2\cdot$	$1.21 \times 10^{-11} \exp(444/T)$	
$OH\cdot$ + isoprene → $0.6RO_2\cdot$ + 0.4MVK+MACR	$2.38 \times 10^{-1}1 \exp(357/T)$	
$OH\cdot$ + toluene → $RO_2\cdot$	$1.81 \times 10^{-12} \exp(280/T)$	
$OH\cdot + SO_2 \rightarrow SO_4$	1.50×10^{-12}	
O_3 + α-pinene → $RO_2\cdot$	$6.30 \times 10^{-16} \exp(-580/T)$	
O_3 + β-pinene → $RO_2\cdot$	$1.20 \times 10^{-15} \exp(-1300/T)$	
O_3 + isoprene → $0.6RO_2\cdot$ + 0.4MVK+MACR	$1.03 \times 10^{-14} \exp(-1995/T)$	
$NO_3\cdot$ + α-pinene → $RO_2\cdot$ + $0.8NO_2$	$1.20 \times 10^{-12} \exp(490/T)$	
$NO_3\cdot$ + β-pinene → $RO_2\cdot$ + $0.3NO_2$	2.50×10^{-12}	
$NO_3\cdot$ + isoprene → $0.95RO_2\cdot$ + $0.3NO_2$ + 0.05MVK+MACR	$3.15 \times 10^{-12} \exp(-450/T)$	
Heterogeneous reactions		

$N_2O_5 + H_2O(\ell) \rightarrow 2HNO_3$	$2.67 \times 10^{-7} \times S$ ($\mu m^2\ cm^{-3}$)	Aerosol surface area, S, assumed to be 100 $\mu m^2\ cm^{-3}$
Tuning reactions		
O_3 + wall → 0.65acetaldehyde + 0.12acetone	$1.00 \times 10^{-4}\ s^{-1}$ for A $0.70 \times 10^{-4}\ s^{-1}$ for B	Used to match observed O_3 loss and acetaldehyde and acetone production. Wall "concentration" dependent upon solar intensity to adjust for increase in contact frequency with increased convective mixing.
$OH\cdot + X \rightarrow$	$2\ s^{-1}$	Used to produce reasonable daily peak OH·. Partially constrained by daytime difference between chamber and ambient isoprene resulting from reaction with OH·.
(N_2+O_2) + wall → HONO	$1.0 \times 10^{7}\ s^{-1}$	Recognized radical source in Teflon® chambers. Partially constrained by pattern of daytime difference between chamber and ambient isoprene resulting from reaction with OH·.

- OH· is conserved for all "OH· + reactant →" reactions because an independent overall OH· reactivity is assumed.
- Species in parentheses involved in reaction but not needed for calculated rate.
- Chamber temperature assumed to be the same as ambient temperature.